Monitoring Urban Land Cover in Rome, Italy, and Its Changes by Single-Polarization Multitemporal SAR Images

Fabio Del Frate, *Member, IEEE*, Fabio Pacifici, *Student Member, IEEE*, and Domenico Solimini

***Abstract*—This study contributes an assessment of the potential of single-polarization decametric synthetic aperture radar (SAR) images in classifying land cover within and around large urban areas and in monitoring their changes. The decision task is performed on a pixel basis and is carried out by supervised neural network algorithms fed by radar image features including backscattering intensity, coherence and textural parameters. Two configurations are considered: a short-term classification and change detection scheme intended for providing information in near-real time and a long-term scheme aimed at observing the urban changes at year time scales. We use a pair of interferometric images for the short-term case, while the long-term exercise utilizes two interferometric pairs and a fifth single acquisition. The images are acquired by the ERS SAR in late winter, spring and early summer over 836 square kilometers including Rome, Italy, and its surroundings. The accuracy of the short-term algorithm in discriminating seven types of surface is higher than 86%, while the accuracy of the long-term algorithm is beyond 88%. The many changes undergone by Rome from 1994 to 1999 have been identified by the postclassification comparison change detection procedure. The pixel-by-pixel analysis of the results has been carried out for a 160 square kilometers test area, obtaining a correct detection above 82% (less than 18% missed alarms and 0.3% false alarms).**

***Index Terms*—Change detection, coherence, feature contribution, land-cover classification, neural networks, synthetic aperture radar, texture, urban development.**

I. Introduction

THE global view of urban areas makes satellite missions a valid instrument for updating urban maps and carrying out the analysis of settlement dynamics. Remote sensing in the optical band is a well-established tool for producing maps of urban land use and monitoring changes, but it can suffer from atmospheric limitations, especially where clouds systematically occur or when unpredictable abnormally long periods of cloud cover affect usually clear-sky regions. Hence, when a systematic, timely and reliable survey of an urban area is required, the use of synthetic aperture radar (SAR) imagery [1] might become suitable. Moreover, the management of emergencies over large areas relies on near-real time information, irrespective of the time of day and of the cloud cover: to this purpose the availability of SAR acquisitions is essential.

The C-band SAR data provided in the past decade by the European Space Agency's European Remote Sensing Satellites ERS-1 and ERS-2 and currently ENVISAT, are systematically available at relatively low price. Together with Landsat, they provide a long-term history of the urban areas; hence, their value should not be overlooked. In particular, the long ERS SAR image time series provide a unique systematic means of periodically tracking, retrieving and understanding the frequently dramatic changes undergone by the land cover of large cities in many parts of the world in the past 15 years. The archived radar images also form a database useful to devise and test short-term change detection schemes in a variety of situations. However, the ERS SAR data contain a minimum of information, being at single polarization. Moreover, because of the decametric size of the resolution cells at ground, the shapes of the structures cannot be represented in detail and mixed pixels are likely to occur, especially in a suburban landscape, where heterogeneous land covers coexist within short distances. These limitations bound the potential of data of the ERS type in fully identifying the spatial features of land cover. However, on their side, very-high resolution images may prove unhandy in monitoring very large urban areas, both for the computational burden and for the unnecessary detail they catch. Indeed, for a global characterization of the dynamics of large areas over extended periods of time, images at decametric resolution may often turn out a serviceable compromise. Analogous considerations hold for the near-real time change detection constraint cast by the management of emergencies eventually affecting large cities. In such circumstances, prompt, i.e., irrespective of cloud cover and of time of day, information on the global land cover evolution over large (e.g., hundreds of square kilometers) areas is crucial to the decisional process. The goal of this study is the identification of a set of features of decametric single-polarization SAR images that can be ingested by a readily usable algorithm to yield the all-weather land cover classification of an urban and suburban large area. The method strives to enhance the exploitation of simple SAR systems and reduced data sets in recording urban development. We suggest that the same procedure is applicable to monitor the short-term changes in possible emergencies affecting large towns.

Attaining the goal poses several problems. One concerns the selection of a set of radar image features containing sufficient

Manuscript received October 10, 2007; revised June 19, 2008. First published September 30, 2008; current version published October 15, 2008.

The authors are with the Department of Computer, Systems and Production Engineering (DISP), Tor Vergata University, 00133, Rome, Italy (e-mail: delfrate@disp.uniroma2.it; f.pacifici@disp.uniroma2.it; solimini@disp.uniroma2.it).

Color versions of one or more of the figures in this paper are available at http://ieeexplore.ieee.org.

Digital Object Identifier 10.1109/JSTARS.2008.2002221

information on the types of surface to be discriminated. The second regards the design of a processing algorithm easy to run, able to handle the needed heterogeneous image features and capable to yield the required accuracy.

We propose a method which exploits three different partially independent sources of information carried by a limited set of SAR acquisitions, as might be required in particular events affecting an urban area or to improve the cost-efficiency of the data base. We identify the backscattering intensity, its textural properties, and the interferometric coherence as the set of image features containing the pieces of information embedded both in the amplitude and in the phase of the scattered wave. The minimum number of SAR acquisitions is two, given the need of at least an interferometric image. The short-term (days or possibly less) identification of surface changes utilizes four quantities extracted from the image pair, namely the amplitude of the backscattering coefficient, two textural parameters and the degree of coherence. For the long-term, i.e., interannual, monitoring of the urban dynamics we add the information on the seasonal variations of backscattering and of coherence. A minimum set of five late-winter, early-summer SAR scenes turned out to be suitable for attaining the desired classification accuracy. Now six quantities relative to three types of image features are exploited: the amplitude of the backscattering coefficient averaged over the five images and its standard deviation, the two degrees of interferometric coherence of two pairs of seasonal images, and two backscattering textural parameters. The joint use of these three partially independent SAR image features are a novelty of this study. We point out that most studies on SAR land cover classification do not consider more than two types of image features at the same time [2]–[4].

The decision-making process is performed by a multilayer perceptron (MLP) neural network (NN) supervised classifier [5]. This algorithm satisfies the requirements mentioned above, since, once trained, it runs in real time, has considerable ease in using multidomain data sources, and is able to yield high accuracy. Indeed, the results of a recent data fusion contest indicated that a neural network approach reached the highest accuracy in urban mapping using radar and optical data [6]. Several studies appeared in literature deal with classification of SAR images by neural networks. They mainly refer to crops or forest. In particular, Chen and McNairn [7] reported on rice monitoring using RadarSat-1, while Gimeno *et al.* [8] investigated on burnt areas in the Mediterranean using ERS-2 SAR time series. In both cases, the neural algorithm showed an overall classification accuracy over 90%. The use of SAR data in land-cover classification of urban areas is relatively limited, given the peculiar imaging geometry, the complexity of the interactions between urban features and radar waves and the presence of speckle noise. These effects make generally difficult attaining high classification accuracies by using single-channel single-polarization SAR images. To this end, neural network approaches making use of mean, standard deviation and texture features of the images [2], multiscale textural parameters [3], or backscattering temporal variations and long-term coherence [4] have been worked out.

The paper is organized as follows. The data set is described in Section II. Section III deals with the classification problem, introducing the features used as input to the NN. The design of the neural network is discussed in Section IV. Experimental results of the classification and change detection exercises are reported and accuracies are analyzed in Section V and Section VI, respectively. Discussion and final conclusions follow in Section VII.

TABLE I
DATA SET RELATIVE TO YEARS 1994, 1996, AND 1999. B_p REFERS TO THE PERPENDICULAR COMPONENT OF THE BASELINE

Acquisition Date	Satellite	B_p (m)
January 25, 1994	ERS 1	89
January 31, 1994	ERS 1	
March 26, 1994	ERS 1	157
March 29, 1994	ERS 1	
July 13, 1994	ERS 1	-
February 24, 1996	ERS 1	12
February 25, 1996	ERS 2	
March 30, 1996	ERS 1	106
March 31, 1996	ERS 2	
July 14, 1996	ERS 2	-
February 13, 1999	ERS 1	211
February 14, 1999	ERS 2	
March 20, 1999	ERS 1	65
March 21, 1999	ERS 2	
July 4, 1999	ERS 2	-

II. DATA SET

The study area includes the city of Rome, Italy, and its outskirts for an overall extension of about 836 square kilometers (992×995 pixels). We used a set of single look complex (SLC) SAR images acquired in winter, early spring and early summer by ERS-1 in 1994 and by the ERS-1/2 tandem mission in 1996 and 1999, with five acquisitions each year as reported in Table I. Since the meteorological and climatic aspects may be relevant for understanding the involved physical phenomena, we acquired the precipitation and wind speed data recorded by Aeronautica Militare Italiana at the Ciampino Airport (South-East Rome). A light rainy period preceded the first winter ERS acquisitions in the years 1994, 1996, and 1999, and the first spring acquisition in 1996, while no precipitation was recorded immediately before the March acquisitions. The measured values of backscattering and coherence do not appear to be affected by the recorded meteorological conditions.

For the long-term classification, each set of five images indicated in Table I yielded the classified map for the corresponding year, while only the two images acquired in March of each year were used in the near-real time classification exercise.

III. CLASSIFICATION PROBLEM

A systematic subdivision of land cover types has been proposed in the CORINE project of the European Environment Agency [9]. The basic land covers (Level 1) include four classes (artificial surfaces, agricultural areas, forests and wetlands), while Level 2 refers to 13 cover types, including also mine and dump sites, pasture areas and costal wetland. Given the peculiarities of the Rome urban area, the purpose of our study, and the use of images at decametric resolution, we chose seven land cover classes, consisting of water surfaces (WS), vegetation (VE), arboreous (FO), asphalt/concrete (AS), industrial/commercial buildings (IB), and high/low density continuous urban

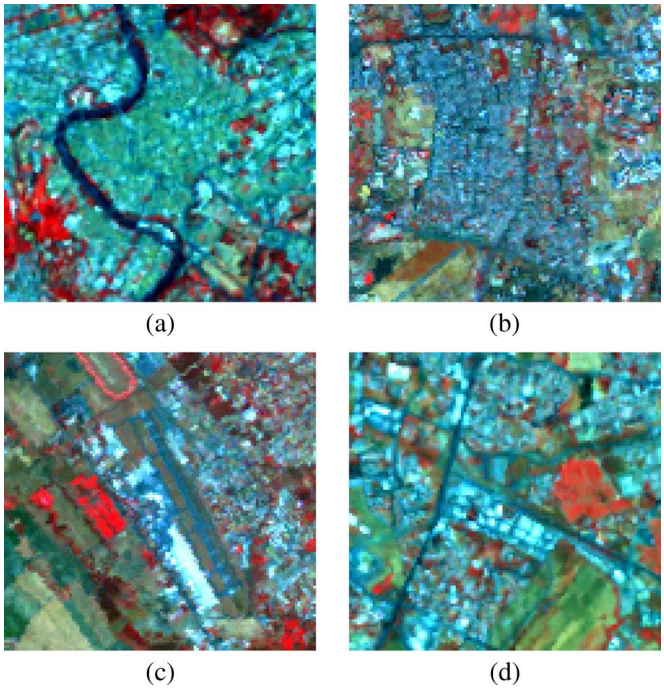

Fig. 1. Landsat false colors composition (Bands 431) of (a) high density continuous urban fabric, (b) low density continuous urban fabric, (c) asphalt/concrete surfaces, and (d) industrial/commercial buildings.

fabric (HD/LD) more suitable to urban analysis. Examples of some of these classes imaged in false colors composition of Landsat bands (RGB 431) are shown in Fig. 1. The high density urban fabric is mainly found in the oldest (middle age to 18th century) sections of the city, while the low density urban fabric is typical of mixed areas with small buildings, gardens and narrow streets with trees, mainly developed in the first half of the 20th century. Asphalted (and concrete) surfaces correspond to large roads, parking lots and airport runways. More recent isolated large residential, commercial, or industrial buildings are found on the borders of the town.

Classification of urban areas by SAR data appeared in literature refers to four [4], five [3], and ten [2] classes. The intent of this paper is to discriminate among the above seven land cover classes utilizing the information stored in the SAR acquisitions; hence, those image features carrying effective information must be identified. The rationale for the choice of the features is discussed in the following.

Urban backscattering typically reaches high values when resulting from single, double-bounce and trihedral reflections from relatively large man-made plane surfaces [2]–[4]. However, the imaging geometry and the structure of the built area, involving the observation azimuth angle and the orientation of buildings, can produce different backscattering values [10]. On the other hand, the backscattering from the man-made structures is only partially sensitive to the different seasons of the year. In contrast, the backscattering intensity of natural (parks) and agricultural areas, which include bare soil and surfaces with trees and low vegetation, may vary significantly with the season, according to the changing geometric (growth, blooming stage and farming activities) and dielectric (moisture) conditions. Hence, when the near-real time response is not required, the seasonal behavior of the backscattering intensity can be also exploited. The first two inputs to the long-term classification algorithm are thus the mean and the standard deviation of the backscattering coefficient σ^0 computed for each pixel over the multitemporal (winter, spring, and summer) data set, while the single-date (spring) intensity only enters the short-term classification algorithm.

The degree of interferometric coherence γ [11] is an indicator of both the temporal and the spatial phase stability of a target according to its geometrical and dielectric proprieties. Coherence has indeed proven useful in land cover discrimination, as reported by several authors [12]–[17]. In particular, Bruzzone *et al.* [4] found that the coherence features proved to increase the classification accuracy by more than 16% when added to a multitemporal data set. They pointed out the effectiveness of coherence to significantly reduce the confusion between both forest and urban areas and fields and urban areas. In fact, in a high-density urban environment, given the stability of man-made structures, coherence is generally high, while low-density residential areas, where gardens and small parks can cover a considerable portion of the surface, exhibit lower coherence.

We assumed the winter and late spring/summer interferometric short-term (one day repeat-pass in 1996 and 1999 or three days in 1994) coherence as the third and the fourth input of our long-term classification scheme, while only the spring value was used for the short-term classification. We point out that several authors highlighted the importance of the long-term coherence, showing the higher accuracy with respect to the short-term coherence in classifying urban land-cover. In fact, for long acquisition time intervals, stable permanent scatterers show high coherence values: in temperate regions, almost exclusively buildings and man-made structures are such stable targets, as reported in [17]. However, the use of long-term coherence is not appropriate for early (near-real time, ideally) operations. In the following, we focus onto the analysis of the accuracy attainable by including only one or two short-term coherence images into the classification algorithm, also in view of possible immediate actions for disaster management. In this case, only single-pass or short-term measurements, as the one reported in [18] or those foreseen by the new-generation satellite constellations, are usable.

The last two inputs to the algorithm have been computed from textural features of the intensity image [19]. Many texture features exist, as attested by the numerous papers appeared in literature; hence, reporting some details on the rationale of the choice can be appropriate. Tuceryan and Jain [20] identify four major categories for texture features: statistical (such as those based on the computation of the gray-level co-occurence matrix, GLCM), geometrical, model-based (Markov random fields, MRFs), and signal processing. It was pointed out by Shanmugan *et al.* [21] that textural features derived from GLCM are the most useful for analyzing the contents of a variety of imagery in remote sensing, while, according to Treitz *et al.* [22], statistical texture measures are more appropriate than the geometrical ones in land cover classification. Clausi *et al.* [23] demonstrate that the GLCM method has an improved discrimination ability relative to MRFs with decreasing window size. Indeed, GLCM is

TABLE II
NUMBER OF SELECTED SAR IMAGES, INPUTS AND PARAMETERS USED FOR THE LONG- AND SHORT-TERM SCHEME

Scheme	SAR Images	Inputs	Parameters
Long-term	5	6	Mean Int.
			Int. St. Dev.
			Winter Coh.
			Spring Coh.
			Contrast
			Energy
Short-term	2	4	Mean Int.
			-
			-
			Spring Coh.
			Contrast
			Energy

widely accepted and several studies have used it for land cover classification with SAR data [24]–[26]. We use GLCM to characterize the stochastic properties of the spatial distribution of grey levels in the intensity images. Six GLCM parameters are considered to be the most relevant [27] among the 14 ones that can be computed, some of which are strongly correlated with each other. In their investigation, Baraldi and Parmiggiani [28] concluded that *energy* and *contrast* are the most significant parameters to discriminate between different textural patterns.

To further investigate on textural features, we considered two additional textural parameters, the *Large Number Emphasis* and the *Second Moment* suggested by [29]. These two latter features, *energy* and *contrast* have been computed from our backscattering images. In particular, two different methods (reported in [19] and [30]) were used to generate the *energy* and *contrast* features. The computations have been performed with varying window size (7×7, 11×11, and 15×15 pixels) and for different gray levels (16, 32, 64), thus generating a total of 54 texture images. The class separability has been subsequently computed for the textural images based on the Wilk's lambda as reported in [31]. The two parameters which yielded the maximum value are *energy* and *contrast* (consistently with [19]), with a window size of 7×7 pixels and 16 gray levels as inputs to the classification algorithm. We observe that the texture *energy* is especially valuable in separating high-density from low-density residential areas and asphalt from water, while the texture *contrast* contributes to solving the ambiguity between low vegetation and low-density residential.

To summarize, the classification scheme exploits average and standard deviations of backscattering intensity, coherence and average textural parameters computed by formulas known in literature, e.g., [4] and [19]. To further increase the clarity of the input features, reported in Table II is the number of SAR images and the parameters used for the short-term and the long-term classification schemes, while an example of data input relatively to 1994 is illustrated in Fig. 2.

IV. NEURAL NETWORK DESIGN

As discussed in the previous section, we use three different sources of information, contributing heterogeneous inputs to the classification algorithm. Since these inputs are obtained by applying nonlinear operators to the images, they possess a complicated joint probability distribution; hence, parametric classifiers (such as maximum likelihood) become hard to handle, given the difficulty in reasonable assumptions on the features statistics. Neural networks, which do not require any specific probabilistic assumptions for the class distribution can turn out serviceable. We designed a classification algorithm based on a multilayer perceptron (MLP), a net widely used in solving decision-making problems for a variety of remote sensing applications [32]. The MLP maps the input vector containing the features described in the preceding section onto the output vector containing the land cover classes. The MLP topology has been determined through an optimization of the number of hidden layers and units, based on results appeared in literature, on previous experience and on a specific numerical analysis. Two hidden layers has been found an optimal choice for several land cover applications [33]. We recorded the classification accuracies yielded by a varying number of hidden neurons, starting from a small topology (6-12-12-7) to end with a large one (6-100-100-7). The variance of the accuracy for different initializations of the weights was also computed to monitor the stability of the algorithm. The configuration that maximized the accuracy without indication of instability was retained.

A pruning procedure has then been applied to thin the net. Pruning has several advantages, including reduction of runtime and memory, improvement of the generalization capability and selection of inputs [34]. The fully connected NN has been pruned by the magnitude based pruning (MBP) [35] through an automatic procedure. Although this method is very simple, it rarely yields worse results than algorithms such as optimal brain damage (OBD), optimal brain surgeon (OBS) or skeletonization [36]–[38]. Training of the algorithm was carried out by the scaled conjugate gradient method [39].

The selection of pixels both for the training and testing phases is particularly critical: on one side, the training process impacts on the performance of the algorithm and, on the other, a biased test set can lead to fallacious evaluation of the results. The training samples have been mainly selected by visual inspection of co-registered optical imagery taken by the Landsat 5/7 satellites in 1991 and in 2001, a time range which encompasses the dates of the radar images. Periodically updated ground truth records and cadastral maps have added the information for a reasonably accurate identification of the land cover changes possibly occurred at the times of the SAR acquisitions. Moreover, we used subsequent very-high resolution (QuickBird) multispectral imagery and *in situ* inspections to identify or validate ambiguous ground truth. Since the overall areas of the different surface types differed considerably (e.g., water is much less abundant than urban fabric), care was exerted in including a balanced number of pixels belonging to the each class. To ensure a balanced representation of all classes, we adopted a stratified random sampling (SRS) [40], a widely used strategy which allows the inclusion of samples also of the less likely classes. Therefore, we first selected polygons of the Landsat images such that all surface types were represented, then we randomly picked up individual pixels within each polygon, avoiding correlated neighbouring pixels and preserving the statistical significance of each class. The selection of the independent test set was carried out in an analogous way, including also whole polygons. Table III reports the number of pixels of each class that were selected for the training and validation sets (respectively

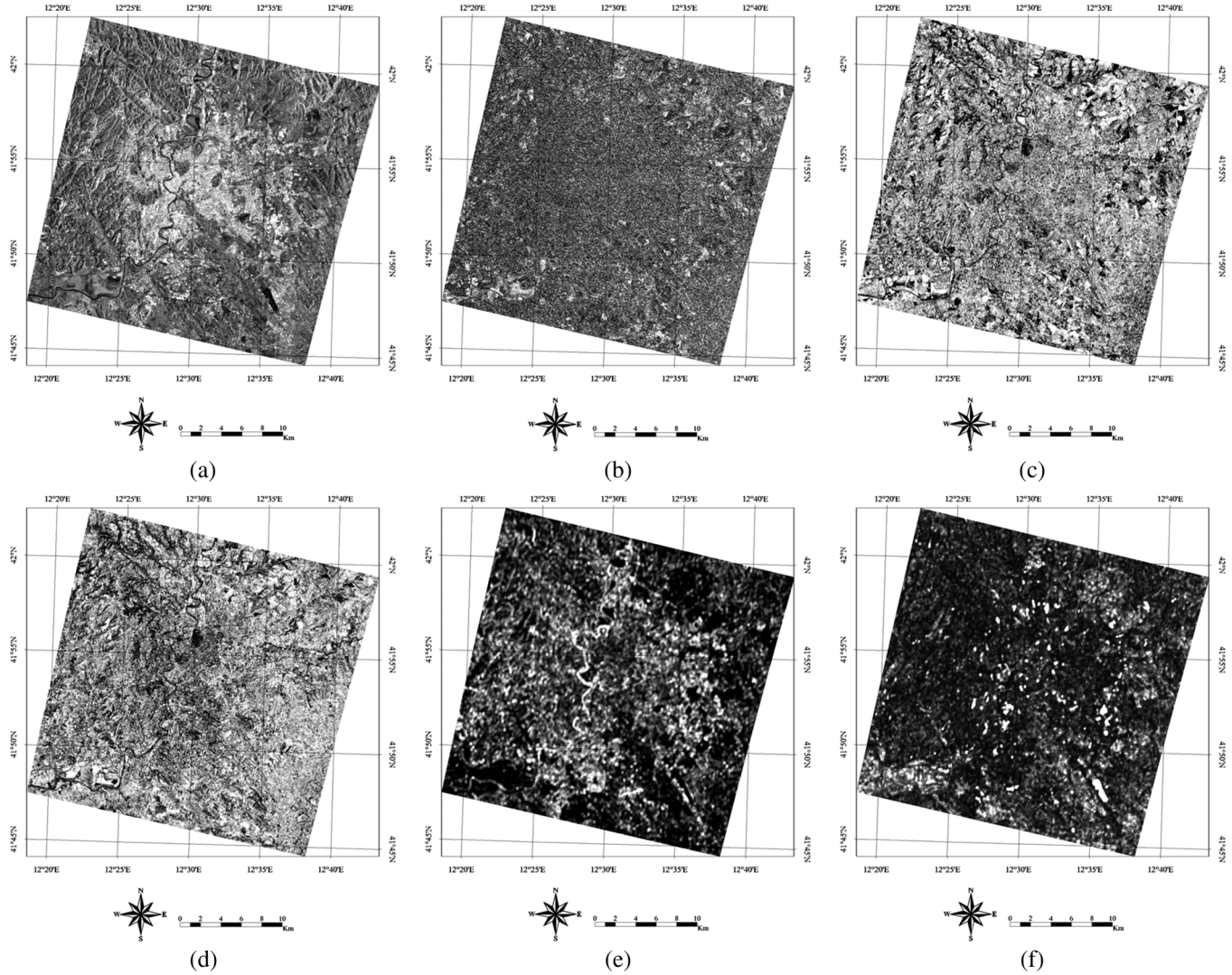

Fig. 2. Six features used as input of the long-term classification algorithm: (a) mean intensity, (b) intensity standard deviation, (c) winter coherence, (d) spring coherence, (e) contrast, and (f) energy for year 1994.

TABLE III
NUMBER OF SELECTED TRAINING (TR) AND VALIDATION (VS) SAMPLES PER CLASS

	Output Classes	TR	VS
1	Asphalt/Concrete (AS)	511	219
2	Forest (FO)	2592	1326
3	High Density (HD)	648	278
4	Industrial Buildings (IB)	122	433
5	Low Density (LD)	4900	6130
6	Vegetation (VE)	3535	6008
7	Water Surfaces (WS)	892	382
	Total pixels	13200	14776

illustrated in Fig. 3). The neural nets were trained by 13200 total samples and the classification accuracy evaluated on 14776 samples selected independently from the training ones.

To further investigate on the influence of the number of both training and test pixels on the results, sets of different size were considered. In addition, the sets were exchanged, in order to use the validation set as training and vice versa. These results are reported in the next section. Here, we highlight that both short-term and long-term classifications have been carried out with algorithms trained and tested by the largest sets, while the effect of the training and test sizes has been studied for the long-term case.

V. CLASSIFICATION RESULTS

We processed the SAR images acquired in 1994, 1996, and 1999 by the algorithm detailed in the preceding section to obtain the classification of the Rome land cover.

The accuracy of the short-term classification, utilizing only the two March images, ranges from 92.0% ($k-\text{Coeff.} = 0.86$) for 1994 to 86.5% ($k-\text{Coeff.} = 0.78$) for 1996 to 89.3% ($k-\text{Coeff.} = 0.83$) for 1999. The addition of the seasonal information by a second interferometric pair and a fifth single image increases the respective accuracies of the (long-term) classifications to 96.0 ($k-\text{Coeff.} = 0.92$) for 1994, 88.0% ($k-\text{Coeff.} = 0.81$) for 1996, and 94.0% ($k-\text{Coeff.} = 0.91$) for 1999.

The figures slightly vary when reducing the number of pixels in the training and test sets. The 1994 long-term classification reaches an accuracy of 95.7% ($k-\text{Coeff.} = 0.94$) when trained on 3507 and tested on 5733 samples; exchanging the sets yields

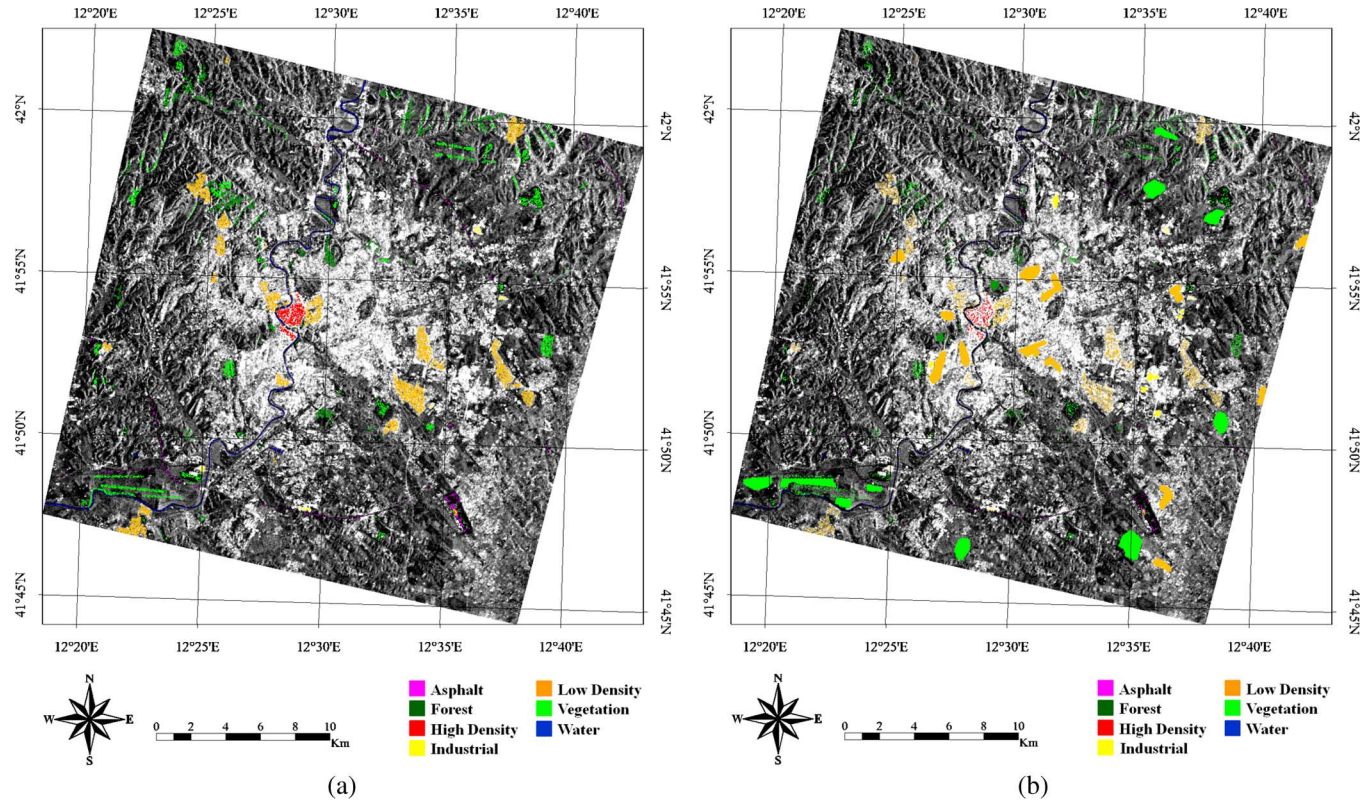

Fig. 3. (a) Training and (b) validation sets superimposed to the mean intensity image of 1999.

93.2% $(k-\text{Coeff.}=0.91)$. Analogously, training on 8182 and testing on 13376 samples lowers the 1999 long-term classification accuracy to 93.5% $(k-\text{Coeff.}=0.91)$; exchanging the sets yields 92.2% $(k-\text{Coeff.}=0.89)$. Taken into account the variability of the surface from year to year, which ensues from the single seasonal evolution and from the meteorological conditions in the days preceding the SAR acquisitions or during them, the above figures seems to confirm the essentially consistent performance of the algorithm, within its expected numerical fluctuations.

The 1994 and 1999 land-cover maps of the Rome area classified by the long-term algorithm are shown in Fig. 4(a) and (b), respectively. In both cases, the main large built area has been identified, as well as some specific structures, such as the compact old part of the city, observable in red in the central part of the images, the Tiber river, the Ciampino airport (in black near the bottom-right corner) and the parks inside the city. The detailed performance of the algorithm in discriminating the considered types of land cover can be appreciated by the confusion matrix shown first for the 1994 short-term case in Table IV. Each row of the matrix refers to a class and shows the probability (in percent) that the corresponding type of surface is attributed to the class shown in the column header. As expected from physical considerations, the classification errors mainly consist in misclassification between high- and low-density continuous urban fabric, between asphalt/concrete and low vegetation, and between parks and low-density residential areas or low vegetation. It can be noted from the confusion matrix in Table V (relative to the 1994 long-term case) that the accuracy improves when using six rather than four parameters, i.e., when including winter coherence and standard deviation of the backscattering coefficient in the classification. This could be expected, since the long-term classification algorithm utilizes a richer input data set. Moreover, the amplitude and texture parameters are now averaged over five images rather than over just two, which results in a more stable estimation of their mean values. Hence, the increase of accuracy is a consequence of the combined effect of adding another coherence image, another amplitude image and of the averaging. As before, misclassification mainly occurs between high-density and low-density urban fabrics, but misclassification between parks and low-density residential areas, as well as between asphalt/concrete and low vegetation, appears mitigated.

An interesting point is the assessment of the relevance of the six partially independent channels in the classification scheme. Several approaches to the quantitative evaluation of the relative information content of an input have appeared in literature, e.g., [41]–[44]. We base the analysis on the concept that input units whose weighted connections have the larger absolute value w are the most important, according to [45]. In the case of two hidden layers, the contribution of an input feature i with respect to a single class j, S_{ij}, is given by

$$S_{ij}=\sum_{k\in H1}\left[\frac{|w_{ik}|}{\sum_{k'\in H1}|w_{ik'}|}\cdot\sum_{x\in H2}\left(\frac{|w_{kx}||w_{xj}|}{\sum_{x'\in H2}|w_{kx'}|\cdot\sum_{x'\in H2}|w_{x'j}|}\right)\right] \quad (1)$$

where $H1$ and $H2$ denote the first and the second hidden layer, respectively. The contribution of an input feature i with respect

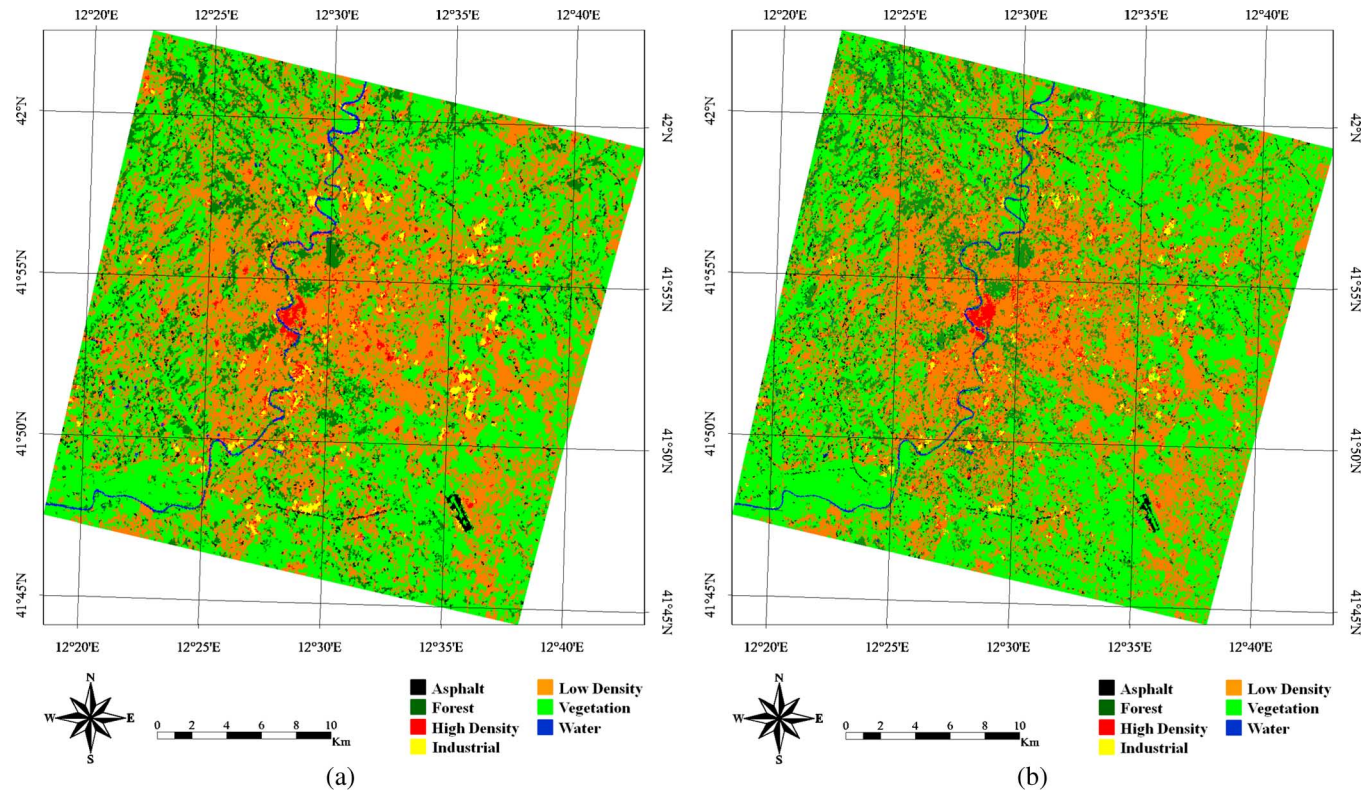

Fig. 4. Long-term classification map for year (a) 1994 and (b) 1999: the main large built area has been identified with good accuracy, as well as some specific structures, such as the compact old part of the city, observable in red in the central part of the image, the Tiber river, the Ciampino airport (near the bottom-right corner), and the parks inside the city.

TABLE IV
SHORT-TERM CLASSIFICATION: CONFUSION MATRIX FOR YEAR 1994

	AS	FO	HD	IB	LD	VE	WS
AS	74.18	2.75	0.00	0.00	0.00	19.23	3.85
FO	0.00	81.39	0.00	0.00	16.71	10.05	1.49
HD	0.00	0.00	36.32	1.42	61.32	0.94	0.00
IB	0.00	0.00	1.12	96.21	2.68	0.00	0.00
LD	0.07	0.95	0.23	0.11	96.99	1.65	0.00
VE	0.39	1.08	0.00	0.00	7.66	93.50	0.01
WS	1.22	1.52	0.00	0.00	0.30	0.30	93.92
	Overall Error= 8.12%					k-**Coef**= 0.863	

TABLE V
LONG-TERM CLASSIFICATION: CONFUSION MATRIX FOR YEAR 1994

	AS	FO	HD	IB	LD	VE	WS
AS	94.51	0.00	0.00	0.55	0.55	4.40	0.00
FO	0.00	93.07	0.00	0.00	2.85	3.80	0.27
HD	0.00	0.00	87.74	0.00	11.32	0.94	0.00
IB	0.00	0.00	3.35	93.75	2.68	0.22	0.00
LD	0.00	0.34	1.67	0.08	95.39	2.52	0.00
VE	0.43	2.47	0.00	0.15	1.80	95.16	0.00
WS	0.00	0.30	0.00	0.00	0.00	0.00	96.96
	Overall Error= 4.01%					k-**Coef**= 0.923	

to the all output classes, S_i, is defined as the sum of the S_{ij} values over all classes N_{cl}

$$S_i = \sum_{j=1}^{N_{cl}} S_{ij}. \tag{2}$$

TABLE VI
RELEVANCE OF THE SIX CHANNELS PER SINGLE CLASS

	AS	FO	HD	IB	LD	VE	WS
Mean Int.	0.113	0.156	0.111	0.190	0.210	0.073	0.147
Int. St. Dev.	0.062	0.087	0.059	0.106	0.122	0.037	0.080
Winter Coh.	0.070	0.097	0.070	0.117	0.128	0.047	0.092
Spring Coh.	0.074	0.100	0.075	0.123	0.131	0.048	0.096
Contr.	0.083	0.114	0.080	0.137	0.155	0.054	0.108
Energy	0.096	0.129	0.095	0.161	0.176	0.063	0.126

The feature contribution per single class S_{ij} is reported in Table VI. Globally, the backscattering intensity carries the maximum information, followed by energy, contrast and the two short-term coherence features, while the standard deviation of intensity contributes the least as shown in Fig. 5. This result seems to confirm previous results on urban classification from multitemporal SAR data [4]. The authors reported a classification accuracy of 65% using only temporally filtered images rising to about 81% when the long-term coherence was added (in the present study we exploit short-term coherence). Hence, the contribution of coherence is important, since it increases the overall classification accuracy, but the other features are also quite effective. We point out that our result has been obtained for the particular urban scenario, land cover classes, and SAR acquisitions we consider. However, it suggests that backscattering amplitude and texture might contribute considerable information when classifying areas with abundant urban fabric.

Finally, it is interesting to note that the short-term classification scheme exploits just the four quantities contributing more

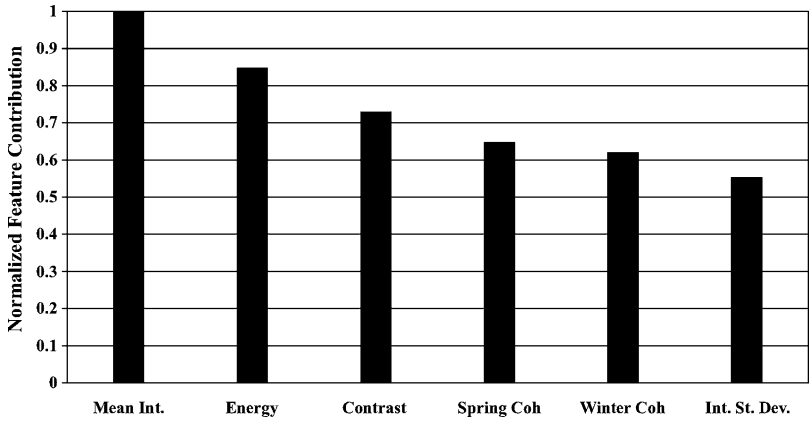

Fig. 5. Normalized feature contribution of the six channels. The backscattering intensity carries the maximum information, followed by the textural energy and contrast, and by the coherence features. The standard deviation of intensity contributes the least.

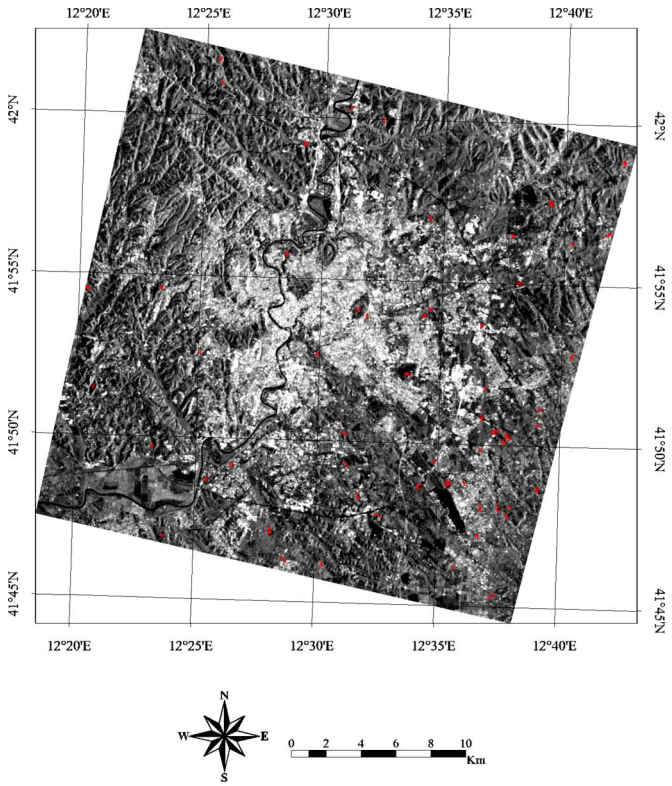

Fig. 6. Change map of the Rome test site produced by post classification comparison of the 1994 and 1999 land cover maps obtained by the long-term algorithm (see Fig. 4). The considered changes (shown in red) are surfaces that transitioned from natural areas to built units. The large-scale changes occurred in the five year time interval show a fast developing urbanization in the eastern side of Rome with the construction of several industrial and residential buildings.

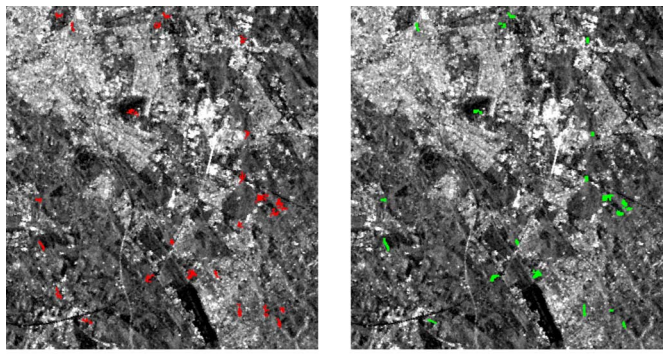

Fig. 7. (a) Detail of Fig. 6 (the changes found with the long-term algorithm are in red), including the South-East side of Rome which underwent considerable land surface changes before the Jubilee in 2000; (b) relative ground truth record (shown in green). The correct detection of the long-term algorithm is slightly above 82%, about 18% missed alarms and 0.3% false alarms.

information, although the contribution of the winter coherence is quite close to that of the spring one.

VI. Change Detection

Several results have appeared in literature regarding urban classification by multitemporal SAR data at decametric resolution (nonexhaustive examples are [3], [4], [10], [16], [46]); however, only a few deal with urban change detection. Grey *et al.* [10] exploited a multitemporal sequence of ERS interferometric coherence data for mapping urban changes in Cardiff (U.K.), reaching approximately 50% of accuracy in detecting the building developments occurred within their test site. The authors report that, while the large developments can be accurately identified, many of the smaller developments are not detected in the binary change map.

As discussed previously, the intent of this paper is the monitoring of changes within and around large urban areas. To this end, the classification results detailed in the previous section are now utilized for an extended-area postclassification comparison change detection. The changes underwent by the Rome area are the ones typical of a developing urbanization, i.e., from natural surface to industrial, commercial and residential buildings. For this reason, we only investigate on surfaces that transitioned to built units as in [10]. We consider the classified images of 1994 and 1999 in order to have a significant number of changes available for the analysis.

The pixel-by-pixel comparison of the two yearly land cover maps obtained by the long-term algorithm yields the large-scale changes occurred in the five year time interval. Fig. 6 shows the detected several hundreds of occurrences scattered over the 836 km^2 Rome's urban and suburban area superimposed on the 1994 Mean Intensity background without changes. The higher density of changes appears on the eastern side of the area. A detailed analysis of the changes detected in the North East corner,

TABLE VII
LONG-TERM CHANGE DETECTION ACCURACY

Correct Detection	Missed Alarm	False Alarm
82.17%	17.83%	0.26%

where topography is apparent, revealed that most of them are real modifications associated with major public works, housebuilding and lanscaping. They include the construction of a high speed railroad, a technology park, the new general market, residential sites, and a golf course. The maximum height in this area is about 100 m above sea level. Rather, the higher slopes are located on the western side of the central urbanized area, where the top of the city, Monte Mario, attains 139 m. This high-slope area, on the west side of the river, does not show changes. An even higher density of changes appears in the SE corner. Here the territory gently rises towards the Colli Albani mountains with moderate slopes and some fairly flat areas, like the quite visible Ciampino airport. For a quantitative analysis of the results, we refer to this area [shown in Fig. 7(a)] having an extension of about 160 km^2 (423 $\times$ 465 pixels), which underwent considerable land surface changes and for which we have a particularly detailed independent ground survey [shown in Fig. 7(b)].

The correct detection is slightly above 82%, with about 18% missed alarms and 0.3% false alarms, as reported in Table VII.

The short-term change detection is suitable for mapping the surface modifications caused by particular natural events like flooding or earthquake. In these occurrences the typical changes are from solid surface to water or from buildings to a mixture of man-made and rough surfaces. Although some example can be found in particular locations [40], such changes are extremely uncommon in the normal evolution of a city like Rome. Hence, the results of the change detection based on the short-term classifications should not be regarded as representative of the performance of the technique in such possible natural events, rather only indicative of its potential. The pixel-by-pixel comparison of the 1994 and 1999 land cover maps produced by the short-term (4 inputs) data set of the test area yields a correct detection slightly above 62%, with about 38% missed alarms and 0.2% false alarms. These results show an improvement with respect to the urban change detection accuracy reported in literature ([10]).

VII. SUMMARY AND CONCLUSION

The global dynamics of large urban areas is hard to monitor by images at metric spatial resolution. Moreover, the short reaction time allowed by emergencies makes radar acquisitions an essential element of the decision-making process. The archived ERS SAR images, on one side provide a valuable source of information on the evolution of human settlements and urban land use, and, on the other, are a tool for preparing and testing readily employable change detection techniques. We explored the potential of single-polarization decametric SAR data in both applications by discussing the extraction of suitable features and by using them in producing land cover maps through a neural network algorithm to arrive at a postclassification change detection. The study refers to a wide area of more than 800 km^2, including the city of Rome, Italy, which was imaged in three different years between 1994 and 1999.

A novelty of this study is the joint use of intensity, coherence and texture of SAR images, which were exploited separately in previous studies. The NN algorithm behaves quite satisfactorily in handling such an heterogeneous data set and in yielding reasonable results. However, the algorithm requires care in designing its topology (number of hidden layers and units), in scaling input and output quantities, and in training and pruning procedures. Once optimized and trained, the Neural Net can classify large amounts of data in quite short times. Moreover, it can provide indication on the information that each image feature carries on the considered land cover classes. Backscattering intensity, GLCM energy and contrast, and spring coherence turned out to be the most effective parameters in classifying the particular landscape at hand.

The accuracy in discriminating the considered seven types of surface from a single interferometric acquisition exceeded 86%, with a k-Coeff. larger than 0.78. Including different seasons by acquiring a second interferometric image pair and by adding a fifth image, rose the accuracy to beyond 88% (k-Coeff. above 0.80). The influence of the number of both training and validation samples on the classification accuracy was investigated. The results confirm the essentially consistent performance of the algorithm, within its expected numerical fluctuations.

The postclassification change detection pointed out the multitude of changes from natural surfaces to buildings that Rome experienced in the five considered years. Several changed sub-areas were analyzed in detail also by very-high resolution (QuickBird) multispectral images and, by *in situ* inspections when needed. The quantitative assessment carried out on the test area, which is a considerable fraction of the whole image, yields a minimum correct detection above 82% (less than 18% missed alarms and 0.3% false alarms). The case of short-term change detection has also been considered, by utilizing a single interferometric image pair. The reduction of the input features lowers the postclassification change detection accuracy over the test area to 62% (38% missed, 0.2% false alarms), but the accuracy is still higher than the ones previously reported. These figures may not be significant for a natural disaster occurrence, when short-term changes are mainly expected to be solid land to water or building to rough surfaces. In this case a considerably higher accuracy can be expected, given the good performance of the short-term algorithm in discriminating water and buildings from land surfaces. It should be pointed out that short-term monitoring needs images as they become available, without any preliminary screening. This implies the use of backscattering and coherence values measured in possible windy, wet or even rainy conditions. A measurement set also including adverse meteorological situations, as in this study, would be suitable to train the algorithms to use in this eventuality.

This study, carried out for the city of Rome, Italy, is expected to be indicative of the results obtainable for urban areas having similar structure and types of surface, as, at least, may be the case of other European cities.

ACKNOWLEDGMENT

The authors would like to thank F. Ferri and E. Bonci for starting this study with their graduation thesis works and J. Lichtenegger for his support and M. Chini for helpful

discussions. The ERS-1 and ERS-2 data have been made available by ESA through CAT-1 project n. 1368. The Landsat images were provided by Global Land Cover Facility.

REFERENCES

[1] C. J. Oliver and S. Quegan, *Understanding Synthetic Aperture Radar Images*. Norwood, MA: Artech House, 1998.

[2] Y. Ban and H. Hu, "RADARSAT fine-beam SAR data for land-cover mapping and change detection in the rural-urban fringe of the greater toronto area," presented at the Urban Remote Sensing Joint Event, Paris, France, Apr. 11–13, 2007.

[3] F. Dell'acqua and P. Gamba, "Discriminating urban environments using multiscale texture and multiple SAR images," *Int. J. Remote Sens.*, vol. 27, no. 18, pp. 3797–3812, Sep. 2006.

[4] L. Bruzzone, M. Marconcini, U. Wegmüller, and A. Wiesmann, "An advanced system for the automatic classification of multitemporal SAR images," *IEEE Trans. Geosci. Remote Sens.*, vol. 42, no. 6, pp. 1321–1334, Jun. 2004.

[5] C. Bishop, *Neural Networks for Pattern Recognition*. New York: Oxford Univ. Press, 1995.

[6] F. Pacifici, F. Del Frate, W. J. Emery, P. Gamba, and J. Chanussot, "Urban mapping using coarse SAR and optical data: Outcome of the 2007 GRSS data fusion contest," *IEEE Geosci. Remote Sens. Lett.*, vol. 5, no. 3, pp. 331–335, Jul. 2008.

[7] C. Chen and H. McNairn, "A neural network integrated approach for rice crop monitoring," *Int. J. Remote Sens.*, vol. 27, no. 7, pp. 1367–1393, Apr. 2006.

[8] M. Gimeno, J. San-Miguel-Ayanz, and G. Schmuck, "Identification of burnt areas in Mediterranean forest environments from ERS-2 SAR time series," *Int. J. Remote Sens.*, vol. 25, no. 22, pp. 4873–4888, Nov. 2004.

[9] [Online]. Available: http://reports.eea.europa.eu/COR0-landcover/en

[10] W. M. F. Grey, A. J. Luckman, and D. Holland, "Mapping urban change in the UK using satellite radar interferometry," *Remote Sens. Environ.*, vol. 87, no. 1, pp. 16–22, Sept. 2003.

[11] M. Born and E. Wolf, *Principles of Optics*. London, U.K.: Pergamon, 1959, Cap. X..

[12] U. Wegmuüller and C. L. Werner, "SAR interferometric signatures of forest," *IEEE Trans. Geosci. Remote Sens.*, vol. 33, no. 5, pp. 1153–1161, Sep. 1995.

[13] U. Wegmuüller and C. L. Werner, "Farmland monitoring with SAR interferometry," in *Proc. IEEE Geosci. Remote Sensing Symp.*, Florence, Italy, Jul. 10–14, 1995, vol. 1, pp. 544–546.

[14] T. Castel, J. M. Martinez, A. Beaudoin, U. Wegmüller, and T. Strozzi, "ERS INSAR data for remote sensing hilly forested areas," *Remote Sens. Environ.*, vol. 73, pp. 73–86, 2000.

[15] E. Weber and H. A. Zebker, "Penetration depths inferred from interferometric volume decorrelation observed over Greenland Ice Sheet," *IEEE Trans. Geosci. Remote Sens.*, vol. 38, no. 6, pp. 2571–2583, Nov. 2000.

[16] M. E. Engdahl and J. M. Hyyppä, "Land-cover classification using multitemporal ERS-1/2 InSAR data," *IEEE Trans. Geosci. Remote Sens.*, vol. 41, no. 7, pp. 1620–1628, Jul. 2003.

[17] T. Strozzi, P. B. G. Dammert, U. Wegmüller, J. M. Martinez, J. I. H. Askne, A. Beaudoin, and M. T. Hallikainen, "Landuse mapping with ERS SAR interferometry," *IEEE Trans. Geosci. Remote Sens.*, vol. 38, no. 2, pp. 766–775, Mar. 2000.

[18] M. Santoro, J. I. H. Askne, U. Wegmüller, and C. L. Werner, "Observations, modeling, and applications of ERS-ENVISAT coherence over land surfaces," *IEEE Trans. Geosci. Remote Sens.*, vol. 45, no. 8, pp. 2600–2611, Aug. 2007.

[19] R. M. Haralick, K. Shanmugan, and I. Dinstein, "Textural features for image classification," *IEEE Trans. Syst., Man, Cybern.*, vol. SMC-3, no. 6, pp. 610–621, Nov. 1973.

[20] M. Tuceryan and A. K. Jain, "Texture analysis," in *Handbook of Pattern Recognition and Computer Vision*, C. Chen, L. Pau, and P. Wang, Eds. Singapore: World Scientific, 1993.

[21] K. S. Shanmugan, V. Narayanan, V. S. Frost, J. A. Stiles, and J. C. Holtzman, "Textural features for Radar image analysis," *IEEE Trans. Geosci. Remote Sens.*, vol. GRS-19, no. 3, pp. 153–156, Jul. 1981.

[22] P. M. Treitz, P. J. Howarth, P. J. Filho, and E. D. Soulis, "Agricultural crop classification using SAR tone and texture statistics," *Can. J. Remote Sens.*, vol. 26, pp. 18–29, 2000.

[23] D. A. Clausi and B. Yue, "Comparing cooccurrence probabilities and Markov random fields for texture analysis of SAR sea ice imagery," *IEEE Trans. Geosci. Remote Sens.*, vol. 42, no. 1, pp. 215–228, Jan. 2004.

[24] T. Kurosu, S. Uratsuka, H. Maeno, and T. Kozu, "Texture statistics for classification of land use with multitemporal JERS-1 SAR single-look imagery," *IEEE Trans. Geosci. Remote Sens.*, vol. 37, no. 1, pp. 227–235, Jan. 1999.

[25] L. Kurvonen and M. Hallikainen, "Textural information of multitemporal ERS-1 and JERS-1 SAR images with application to land and forest type classification in boreal zone," *IEEE Trans. Geosci. Remote Sens.*, vol. 37, no. 2, pp. 680–689, Mar. 1999.

[26] S. Arzandeh and J. Wang, "Texture evaluation of RADARSAT imagery for wetland mapping," *Can. J. Remote Sens.*, vol. 28, pp. 653–666, 2002.

[27] R. Cossu, "Segmentation by means of textural analysis," *Pixel*, vol. 1, pp. 21–24, 1988.

[28] A. Baraldi and F. Parmiggiani, "An investigation of the textural characteristics associated with gray level cooccurrence matrix statistical parameters," *IEEE Trans. Geosci. Remote Sens.*, vol. 33, no. 2, pp. 293–304, Mar. 1995.

[29] C. Sun and W. G. Lee, "Neighboring gray level dependance matrix for texture classification," *Comput. Vis., Graph., Image Process.*, vol. 23, pp. 341–352, 1982.

[30] A. Al-Janobi, "Performance evaluation of cross-diagonal texture matrix method of texture analysis," *Pattern Recognit.*, vol. 34, pp. 171–180, 2000.

[31] P. Basili, P. Ciotti, G. D'Auria, F. S. Marzano, N. Pierdicca, and P. Quarto, "Assessment of polarimetric features to discriminate land cover from the MAESTRO 1 campaign," *Int. J. Remote Sens.*, vol. 15, no. 14, pp. 2887–2899, Sep. 1994.

[32] F. Del Frate, A. Petrocchi, J. Lichtenegger, and G. Calabresi, "Neural networks for oil spill detection using ERS-SAR data," *IEEE Trans. Geosci. Remote Sens.*, vol. 38, no. 5, pp. 2282–2287, Sep. 2000.

[33] F. Del Frate, F. Pacifici, G. Schiavon, and C. Solimini, "Use of neural networks for automatic classification from high-resolution images," *IEEE Trans. Geosci. Remote Sens.*, vol. 45, no. 4, pp. 800–809, Apr. 2007.

[34] F. Del Frate, A. Ortenzi, S. Casadio, and C. Zehner, "Application of neural algorithms for a real-time estimation of ozone profiles from GOME measurements," *IEEE Trans. Geosci. Remote Sens.*, vol. 40, no. 10, pp. 2263–2270, Oct. 2002.

[35] T. Kavzoglu and P. M. Mather, "Pruning artificial neural networks: An example using land cover classification of multi-sensor images," *Int. J. Remote Sens.*, vol. 20, no. 14, pp. 2787–2803, 1999.

[36] A. Zell *et al., SNNS, Stuttgart Neural Network Simulator, User Manual v. 4.2*. Stuttgart, Germany: Univ. Stuttgart.

[37] B. Hassibi, D. G. Stork, and G. Wolf, "Optimal brain surgeon and general network pruning," in *Proc. IEEE Int. Conf. Neural Networks*, San Francisco, CA, Apr. 1993, pp. 293–300.

[38] T. Ragg, H. Braun, and H. Landsberg, "A comparative study of neural network optimization techniques," presented at the nt. Conf. Adaptative and Natural Computing Algorithms, Norwich, U.K., 1997.

[39] M. F. Møller, "A scaled conjugate gradient algorithm for fast supervised learning," *Neural Netw.*, vol. 6, no. 4, pp. 525–533, 1993.

[40] M. Chini, F. Pacifici, W. J. Emery, N. Pierdicca, and F. Del Frate, "Comparing statistical and neural network methods applied to very high resolution satellite images showing changes in man-made structures at Rocky Flats," *IEEE Trans. Geosci. Remote Sens.*, vol. 48, no. 6, pp. 1812–1821, Jun. 2008.

[41] R. Batitti, "Using mutual information for selecting features in supervised neural net learning," *IEEE Trans. Neural Netw.*, vol. 5, no. 4, pp. 537–550, Apr., 1994.

[42] T. Cibas, F. F. Soulié, P. Gallinari, and S. Raudys, "Variable selection with neural networks," *Neurocomputing*, vol. 12, pp. 223–248, 1996.

[43] E. Gascoa, J. S. Sanchez, and R. Alonso, "Eliminating redundancy and irrelevance using a new MLP-based feature selection method," *Pattern Recognit.*, vol. 39, pp. 313–315, 2006.

[44] D. G. Gomes, N. Agoulmine, Y. Bennani, and J. Neuman de Souza, "Predictive connectionist approach for VoD bandwidth management," *Computer Commun.*, vol. 30, pp. 2236–2247, 2007.

[45] Y. Bennani and M. Yacoub, "Features selection and architecture optimization in connectionist systems," *Int. J. Neural Syst.*, vol. 10, pp. 379–395, 2000.

[46] F. Dell'Acqua and P. Gamba, "Texture-based characterization of urban environments on satellite SAR images," *IEEE Trans. Geosci. Remote Sens.*, vol. 41, no. 1, pp. 153–159, Jan. 2003.

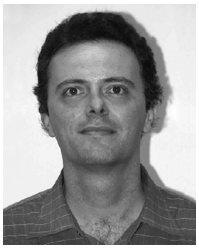

Fabio Del Frate (M'03) received the Laurea degree in electronic engineering in 1992 and the Ph.D. degree in computer science in 1997, both from the Tor Vergata University, Rome, Italy.

From September 1995 to June 1996, he was a Visiting Scientist with the Research Laboratory of Electronics at the Massachusetts Institute of Technology, Cambridge. In 1998 and 1999, he was with the European Space Agency (ESA), ESRIN establishment, Frascati, Italy, as a Research Fellow and was engaged in projects concerning end-to-end remote sensing applications. Currently, he is a Research Professor with the Tor Vergata University, Rome, Italy, where he teaches courses of electromagnetics and neural networks. He has acted and is PI in several remote sensing projects supported by ESA. He is author or coauthor of more than 150 scientific publications, with a special focus on the applications of neural networks to remote sensing inversion problems. His main research topics include retrieval and classification algorithms for land cover from satellite data, oil spill detection in SAR imagery, retrieval of atmospheric variables with microwave radiometry, and data-exploitation for the new missions PROBA and OMI.

Dr. Del Frate serves as a reviewer for different remote sensing journals and as an Associate Editor for the IEEE GEOSCIENCE AND REMOTE SENSING LETTERS.

Fabio Pacifici (S'03) was born in Rome, Italy, in 1980. He received the Laurea (B.S., *cum laude*) and the Laurea Specialistica (M.S., *cum laude*) degrees in telecommunication engineering from the University of Rome Tor Vergata, Rome, Italy, in 2003 and 2006, respectively. He is currently pursuing the Ph.D. degree in geoInformation at the Earth Observation Laboratory, University of Rome Tor Vergata.

Since 2005, he has been collaborating with the Department of Aerospace Engineering Sciences, University of Colorado, Boulder. He is currently involved in various remote sensing projects supported by the European Space Agency and the Italian Space Agency, with special emphasis on neural network applications. His research focus activities include remote sensing image processing, analysis of multitemporal imagery, and data fusion. Particularly, his interests are related to classification and change detection of urban areas using very high-resolution optical and synthetic aperture radar imagery.

Mr. Pacifici ranked first place in the 2007 IEEE GEOSCIENCE AND REMOTE SENSING Data Fusion Contest. He is a reviewer for the IEEE TRANSACTIONS ON GEOSCIENCE AND REMOTE SENSING and the IEEE GEOSCIENCE AND REMOTE SENSING LETTERS.

Domenico Solimini is a full Professor of engineering with the University of Rome Tor Vergata, Rome, Italy.

He has given courses on antennas and propagation (since 1966), remote sensing (since 1975), and electromagnetic fields (since 1979). His remote sensing course was the first of its kind in Italian universities and the GeoInformation Ph.D. he coordinates is an innovative multidisciplinary programme with emphases on Remote Sensing and its applications. He has been Dean of the Electronics Engineering and Environmental Engineering Faculty Councils, has chaired the Computer, Systems and Production Engineering Department, and is Dean of the GeoInformation Ph.D. Faculty Council of the University of Rome Tor Vergata Doctoral School. His research activity has been concerned with lasers, microwave antennas, microwave and millimeter-wave propagation, microwave medical imaging, and passive and active remote sensing of both the Earth's atmosphere and the land surface. He has authored and coauthored over 300 publications, including over 250 papers in refereed international journals, books and conference proceedings. He has been principal investigator and co-investigator of several international remote sensing projects and has coordinated the Concerted Action named European Radar-Optical Research Assemblage (ERA-ORA) within the European Fourth Framework Programme, involving institutions from eight European Countries and the European Space Agency. He acted as a reviewer for several international journals.

Prof. Solimini has been an Italian member of the International Union of Radio Science Commission F and AEI. He has been chairman of the Central and South Italy Section of the IEEE and of the IEEE Geoscience and Remote Sensing Society Chapter. He was the recipient of the 2005 IEEE GRSS Education Award, "in recognition of his significant educational contributions to Geoscience and Remote Sensing." In 2006, he co-founded GEO-K, a high-tech geoinformation company, spin-off of the University of Rome Tor Vergata. He served as General Chairman of the Fourth Specialist Meetings on Microwave Radiometry and Remote Sensing, and has been a member of the Scientific Committees for many conferences.